Single-mode regime of square-lattice photonic crystal fibers

F. Poli, M. Foroni, M. Bottacini, M. Fuochi, N. Burani, L. Rosa, A. Cucinotta, and S. Selleri

Information Engineering Department, University of Parma, Parco Area delle Scienze 181/A, 43100 Parma, Italy

Received December 7, 2004; revised manuscript received January 24, 2005; accepted March 1, 2005

The modal cutoff of square-lattice photonic crystal fibers with a finite number of air-hole rings has been accurately investigated to our knowledge for the first time. By analyzing the leaky behavior of the second-order mode, we have obtained a phase diagram that describes the regions of single-mode and multimode operation as well as the endlessly single-mode regime. Furthermore, starting from these results, we have obtained the cutoff normalized frequency according to two different formulations of the V parameter previously adopted for fibers with a triangular lattice. A final comparison of the cutoff properties of fibers characterized by a square lattice and a triangular lattice has been carried out.

OCIS codes: 060.2310, 060.2340, 060.2400.

1. INTRODUCTION

Photonic crystal fibers (PCFs) are characterized by an array of air holes running along the entire fiber length, which provides for the confinement and guidance of light.[1,2] Owing to the huge variety of air-hole arrangements, PCFs offer many possibilities for controlling the refractive index contrast between the core and the microstructured cladding and, as a consequence, offer novel and unique optical properties.[3] In particular, it has been demonstrated that PCFs with a silica core, which guide light by modified total internal reflection, can be designed to be endlessly single mode (that is, only the fundamental mode can propagate in the fiber core for all wavelengths), unlike conventional fibers that exhibit a cutoff wavelength below which higher-order modes are supported.[4,5] A cutoff analysis for PCFs is not trivial as for conventional optical fibers because all the modes propagating in PCFs with a finite air-hole ring number are leaky.[6–8] The single-mode regime has already been successfully investigated for triangular PCFs with a silica core, obtained by removing the central air hole in the fiber cross section, which are usually described by the hole-to-hole spacing or pitch, Λ, and the ratio d/Λ between the air-hole diameter and the pitch.[5,9–11] In particular, it has been demonstrated that triangular PCFs are endlessly single mode for $d/\Lambda < d^*/\Lambda$, and recently the value $d^*/\Lambda \simeq 0.406$ has been proposed.[10,11]

The aim of the present analysis is to study the cutoff properties of square-lattice PCFs, that is, to investigate the boundary between the single-mode and the multimode operation regimes. In these PCFs, air holes are organized in a square lattice characterized by the same geometric parameters as the triangular ones, Λ and d/Λ, as shown in Fig. 1. Researchers have already demonstrated the technological feasibility of square-lattice PCFs, which can be drawn from intermediate preforms realized with the standard stack-and-draw fabrication process.[12] Recently, square-lattice fibers have been fabricated and characterized in order to analyze their polarization properties, and a great potential for high birefringence has been shown.[13] Promising results have also been obtained by numerically investigating their guiding,[14] dispersion,[15] and polarization[16] properties. Moreover, compared with triangular PCFs,[15] they present a wider effective area for fixed d/Λ and Λ values, so they can be of practical interest as large-mode-area fibers for high-power delivery. In order to successfully use square-lattice PCFs for this kind of application, it is necessary to accurately define their single-mode operation regime.

In this work the cutoff analysis of the square-lattice PCFs has been carried out through a method previously adopted for fibers with a triangular lattice, based on the leaky nature of the second-order mode,[9] and the phase diagram with the boundary between single-mode and multimode regions has been obtained. Results have shown that the endlessly single-mode regime for square-lattice PCFs is a bit wider than that for triangular ones.

Finally, the information about the single-mode regime has been used to evaluate the cutoff value V^* of the normalized frequency V. As in the case of triangular PCFs,[5,11,17] the problem is to properly choose the values of the parameters involved in the definition of V, in particular, the core dimension. In the present analysis, two different definitions of the V parameter have been considered, and the obtained V^* values have been compared with those given for triangular PCFs.

2. THEORETICAL APPROACH

Different approaches have been proposed in previous studies to study the single-mode regime of triangular PCFs, which is the wavelength range where only the first-order mode is guided and the higher-order ones are unbound. In particular, it is necessary to decide clearly at which wavelength λ^* the second-order mode is no longer guided; that is, it becomes a delocalized cladding mode. In order to find this transition, it is possible to take into account the divergence at long wavelengths of its effective

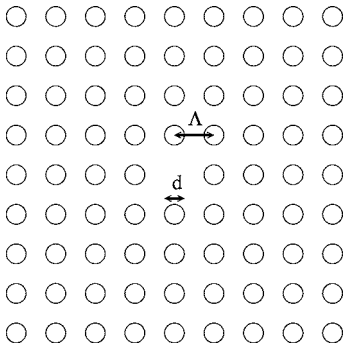

Fig. 1. Cross section of a four-air-hole-ring square-lattice PCF with air-hole diameter d and pitch Λ.

area[18] or its leakage losses, which are related to the attenuation constant α, the real part of the complex propagation constant.[6,8] In particular, the normalized cutoff wavelength λ^*/Λ can be evaluated by observing the transition shown by the behavior of α/k_0, where k_0 is the wave number, versus λ/Λ.[9] This can be made evident by calculating the Q parameter,

$$Q = \frac{d^2 \log[\alpha/k_0]}{d^2 \log(\Lambda)}, \tag{1}$$

because it exhibits a sharp negative minimum at λ^*/Λ.[9] In the present analysis the phase diagram with single-mode and multimode operation for square-lattice PCFs has been obtained by calculating the Q parameter for different normalized wavelengths λ/Λ and by evaluating its negative minima for PCFs with d/Λ in the range of 0.45–0.57. The analysis has been developed by fixing the guided-mode wavelength at 633 nm as well as at 1550 nm. The hole-to-hole distance Λ has been properly selected to obtain the desired normalized wavelength value. Owing to the strong influence of the air-hole ring number on the leakage losses of PCFs with a finite cross section,[6,7] fibers with four, six, and eight rings have been considered for the modal cutoff analysis. In fact, it has been already demonstrated that the transition of the Q parameter becomes more acute and the method more reliable as the ring number increases.[9]

As a second part of the proposed analysis, starting from the single-mode regime information obtained with the Q-parameter approach, we have evaluated the normalized cutoff frequency V^*. The V parameter can be easily calculated in a standard optical fiber, since it depends on the core radius and the core and cladding refractive indices, which are all well defined. The choice of these parameters for PCFs is not trivial, and several formulations of the normalized frequency have been proposed in the literature,[5,11,17,19–21] on the basis of either geometric and physical considerations or analogies with classical theory of conventional fibers. In this study, two formulations of the V parameter are considered. The first one is

$$V_1 = \frac{2\pi}{\lambda}\Lambda\sqrt{n_{\mathrm{eff}}^2 - n_{\mathrm{FSM}}^2}, \tag{2}$$

which has been recently proposed for triangular PCFs.[11,22] In Eq. (2) n_{eff} and n_{FSM} are the effective indices, respectively, of the fundamental guided mode and of the fundamental space-filling mode in the air-hole cladding. The choice of Λ as the effective core radius can be adopted also for the PCFs studied here, since it is the natural length scale of both the triangular and the square lattices.[11,22] The second V-parameter definition here considered, more similar to the one used for conventional fibers, is

$$V_2 = \frac{2\pi}{\lambda}\rho\sqrt{n_{\mathrm{co}}^2 - n_{\mathrm{FSM}}^2}, \tag{3}$$

where n_{co} is the refractive index of the silica core at the operation wavelength and ρ is the effective core radius. For properly adapting the concept of the V parameter to the PCFs, several values for ρ have been proposed in the literature for fibers characterized by a triangular lattice, which are 0.5Λ,[23] $\Lambda/\sqrt{3}$,[20,21] 0.625Λ,[17] 0.64Λ,[19] and Λ.[5,17] In the present study the effective core radius for the square-lattice PCFs has been assumed equal to 0.67Λ. This value, different from all the others previously adopted for triangular PCFs, has been evaluated through the method proposed by Brechet *et al.*[19]

The cutoff value V_1^* here calculated for the square-lattice PCFs has also been compared with the value previously obtained for triangular ones.[11] Then the second-order-mode field distribution has been analyzed in order to extend the approach proposed for triangular PCFs[11] to the square-lattice ones.

Finally, it is important to point out the numerical methods used in this analysis. The complex propagation constants of the fundamental and the second-order modes as well as the field distributions have been calculated by means of a full-vectorial modal solver based on the finite-element method with anisotropic perfectly matched layers.[6,8,24] The multipole method[25,26] has also been used to confirm the simulation results, obtaining a good agreement. The effective index of the mode in the infinite cladding, i.e., the fundamental space-filling mode n_{FMS}, has been evaluated using a freely available software package.[27]

3. RESULTS AND DISCUSSION

In order to calculate the Q parameter according to Eq. (1), one must evaluate the behavior of α/k_0 versus the normalized wavelength λ/Λ for the second-order mode. As shown in Fig. 2, for eight-ring PCFs with different d/Λ values, α/k_0 increases with λ/Λ; that is, the confinement of the second-order mode is lower for smaller pitch Λ. For all the considered d/Λ ratios, the curves show a transition, which is a change in the slope that becomes sharper as the air-hole diameter increases with respect to the pitch. Moreover, when d/Λ is varied from 0.45 to 0.57, the transition region moves toward the higher λ/Λ values, as has already been demonstrated for triangular PCFs.[9] In addition, notice that when $d/\Lambda = 0.45$ it is difficult to identify the transition, which, in contrast, is very sharp when $d/\Lambda = 0.57$. The same behavior of α/k_0 has been obtained for square-lattice PCFs with the lower air-hole ring numbers of four and six. However, it must be observed that, in these cases, as shown in Fig. 3, the transition is not so sharp even for a high d/Λ value.

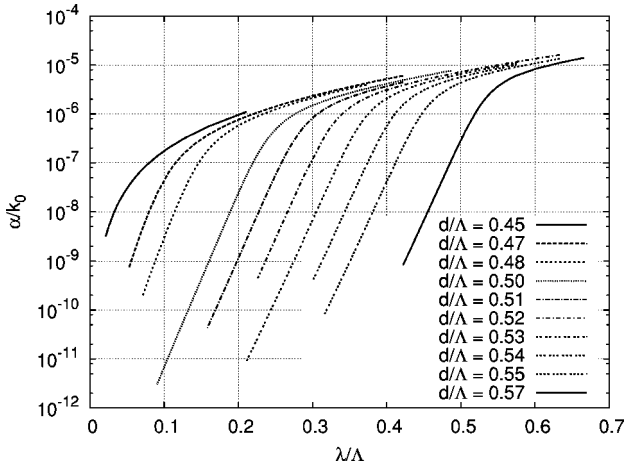

Fig. 2. Second-order mode α/k_0 as a function of the normalized wavelength λ/Λ for eight-ring square-lattice PCFs with d/Λ in the range of 0.45–0.57.

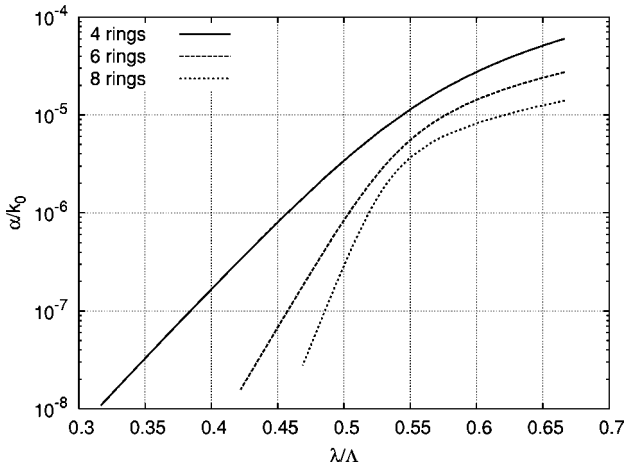

Fig. 3. Second-order mode α/k_0 versus the normalized wavelength λ/Λ as a function of the air-hole ring number, which is four, six, or eight, for a square-lattice PCF with $d/\Lambda=0.57$.

From the previous results, the Q parameter has been calculated through a finite-difference formula, and the values obtained for the eight-ring square-lattice PCFs are reported in Fig. 4. The negative value of the curve minimum becomes higher as d/Λ increases, reaching −654 at $\lambda/\Lambda\simeq0.532$ for $d/\Lambda=0.57$. As the square-lattice PCF air-filling fraction decreases, the Q minimum moves toward the lower λ/Λ values and becomes wide and difficult to identify with high precision. For example, the negative minimum almost disappears for the PCFs with $d/\Lambda=0.45$, and its curve has not even been drawn in the figure. A similar behavior has also been obtained for PCFs with fewer air-hole rings. Figure 5, for example, reports data for PCFs with $d/\Lambda=0.57$, showing that the Q minimum becomes less negative and moves toward higher λ/Λ values when the ring number decreases. In particular, for four-ring fibers the dip is very wide, and the most negative value is only −73 at $\lambda/\Lambda\simeq0.571$, whereas it is −260 at $\lambda/\Lambda\simeq0.541$ when the square-lattice PCFs have six air-hole rings.

In summary, Figs. 2–5 clearly show that when the leakage behavior is strong, whatever the reason, i.e., low d/Λ or few hole rings, it is difficult to define the transition region and the related cutoff wavelength. In contrast, when a high number of hole rings is considered, the slope change in α/k_0 is more evident, the Q curve presents a sharp dip, and it is possible to find reliable values of the normalized cutoff wavelength λ^*/Λ. These values for the square-lattice PCFs with eight air-hole rings are reported in Fig. 6, which also shows data for four- and six-ring PCFs. Notice that the λ^*/Λ values have been reported only for the well-defined and sharp minima, that is, for $d/\Lambda\geq0.48$ for eight-ring PCFs and for $d/\Lambda\geq0.50$ for four- and six-ring PCFs. As expected, results change by increasing the air-hole rings, tending to the values of a PCF with an ideal infinite cladding. This suggests again that the Q-parameter method must be applied assuming a high ring number.

This conclusion is confirmed also by further comments on the obtained results. Looking at Fig. 6, it seems that PCFs with four air-hole rings have a smaller single-mode region, defined by $\lambda/\Lambda>\lambda^*/\Lambda$, their cutoff values being the highest ones. However this result is in contradiction

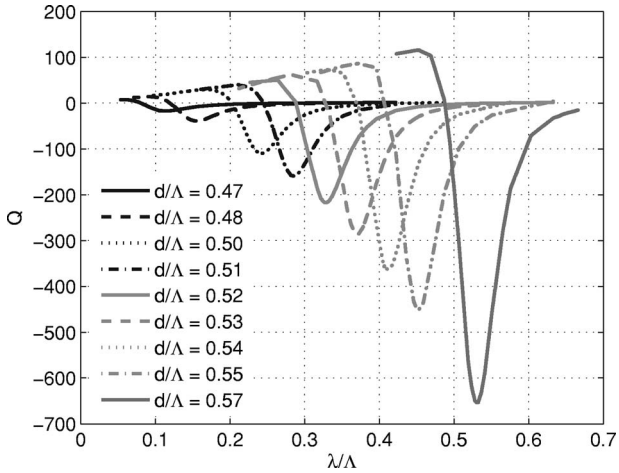

Fig. 4. Q-parameter values as a function of the normalized wavelength λ/Λ for eight-ring square-lattice PCFs with d/Λ in the range of 0.45–0.57.

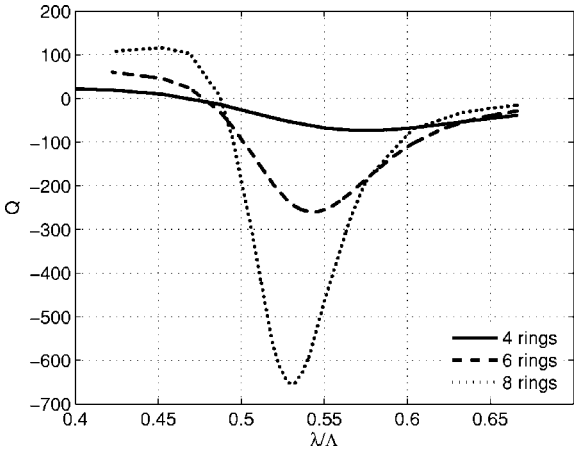

Fig. 5. Q-parameter values versus the normalized wavelength λ/Λ as a function of the air-hole ring number, which is four, six, or eight, for a square-lattice PCF with $d/\Lambda=0.57$.

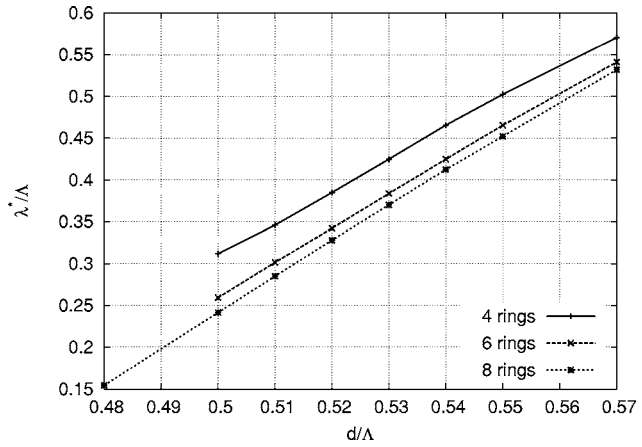

Fig. 6. Normalized cutoff wavelength λ^*/Λ as a function of the d/Λ ratio for square-lattice PCFs with four, six, and eight air-hole rings.

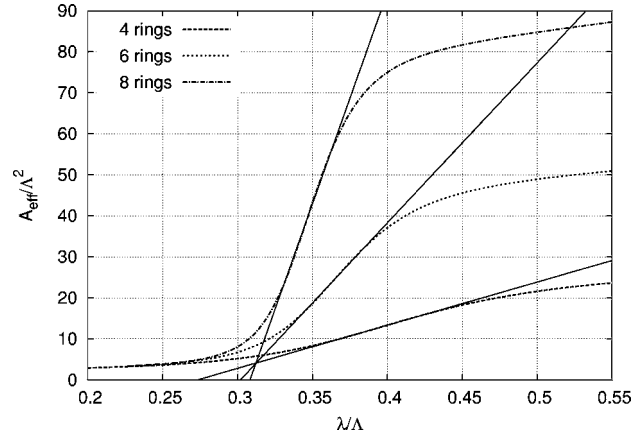

Fig. 7. Second-order-mode normalized effective area A_{eff}/Λ^2 versus λ/Λ for square-lattice PCFs with $d/\Lambda=0.52$ and with four, six, and eight air-hole rings.

with the α/k_0 values reported in Fig. 3, which are also the highest for all the considered λ/Λ. Figure 3, in fact, indicates that the second-order mode suffers from high leakage losses, and, consequently, only the fundamental mode can actually propagate in a wider single-mode spectral range. In other words, the Q-parameter approach fails when a sharp minimum does not occur as shown in Fig. 5 for the case of four air-hole rings. In contrast, when eight hole rings are considered, results are clearly readable and reliable.

It is important to highlight that the λ^*/Λ evaluated for PCFs with many rings of air holes also applies to fibers with few rings in that λ^*/Λ, in any case, is an upper limit of the cutoff wavelength. This means that fibers with a reduced number of rings present an even larger single-mode region.

In order to give a further confirmation of what is stated, the normalized cutoff wavelength has also been evaluated according to another approach, the method based on the second-order-mode effective area proposed by Mortensen.[18] Simulation results for the PCFs with $d/\Lambda=0.52$ are shown in Fig. 7. Notice that the λ^*/Λ values, indicated by the crossing of the solid lines with the horizontal axis, are, respectively, 0.273, 0.302, and 0.308 for the PCFs with four, six, and eight air-hole rings. This means that λ^*/Λ increases with the air-hole ring number; that is, the PCFs that provide the better field confinement have the smallest single-mode operation region and not the other way round as could be suggested by Fig. 6. Moreover, the difference between the normalized cutoff wavelength values almost vanishes if PCFs with six and eight rings are considered.

Thus eight-ring square-lattice PCFs offer the most reliable results and, in the following, will also be used to compare square- and triangular-lattice PCF characteristics.

A first interesting comparison can be made on the endlessly single-mode region. For fibers with a triangular lattice of holes, a fitting of the cutoff curve has been evaluated according to the expression[9]

$$\lambda^*/\Lambda \simeq \alpha(d/\Lambda - d^*/\Lambda)^{\gamma}, \tag{4}$$

where d^*/Λ is the boundary of the endlessly single-mode region, resulting in $d^*/\Lambda=0.406$, $\alpha=2.80\pm0.12$, and $\gamma=0.89\pm0.02$.[9] The same procedure, applied to the λ^*/Λ values of the square-lattice PCFs reported in Fig. 6, provides $d^*/\Lambda\simeq0.442$, $\alpha=4.192\pm0.246$, and $\gamma=1.001\pm0.025$. The boundary between the single-mode and the multi-

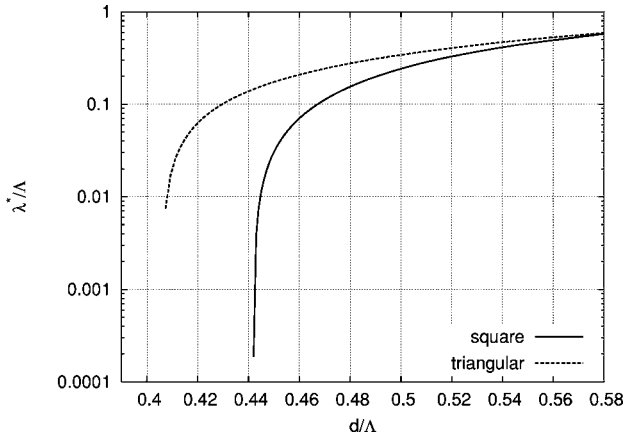

Fig. 8. Phase diagram of the second-order mode for eight-air-hole-ring PCFs characterized by the square and the triangular lattices.

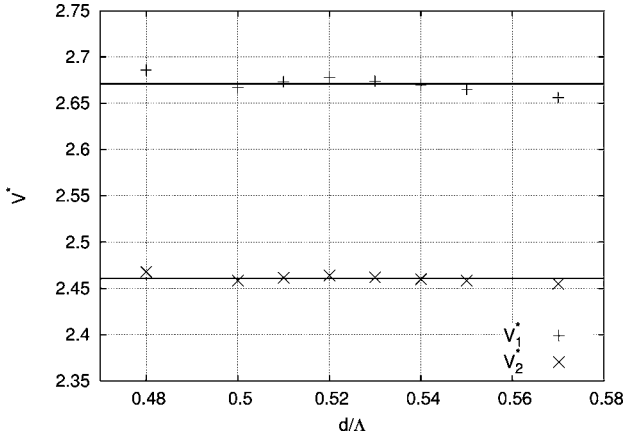

Fig. 9. Cutoff value V^* of the normalized frequency according to the two definitions for square-lattice PCFs with eight rings. Solid lines represent the mean values of V_1^* and V_2^*.

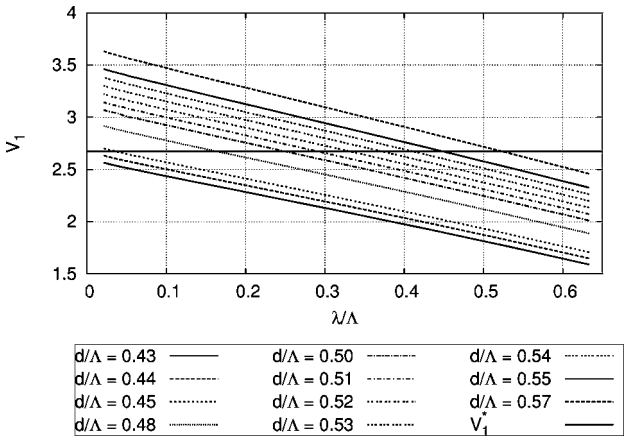

Fig. 10. V_1 behavior versus the normalized wavelength λ/Λ for square-lattice PCFs with d/Λ between 0.43 and 0.57. A solid horizontal line is drawn at the fixed value V_1^*.

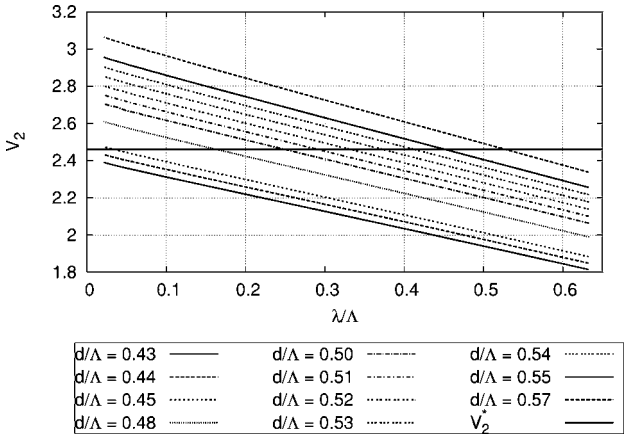

Fig. 11. V_2 behavior versus the normalized wavelength λ/Λ for square-lattice PCFs with d/Λ between 0.43 and 0.57. A solid horizontal line is drawn at the fixed value V_2^*.

mode operation areas is reported in Fig. 8 for square-lattice PCFs and triangular ones. Notice that the single-mode region for square-lattice PCFs, which is the one above the curve in Fig. 8, is wider for lower d/Λ values, but the difference is significantly reduced until it disappears as the air-filling fraction increases. Moreover, it can be noticed that the d^*/Λ value is higher for square-lattice fibers; that is, they can be endlessly single mode in a wider range of the geometric parameter values with respect to triangular PCFs and can be successfully used in applications that need large-mode-area fibers.

A further analysis has been developed on the cutoff value of the normalized frequency. As shown in Fig. 9, V_1^* and V_2^* have been evaluated for the eight-air-hole-ring PCFs, starting from the normalized cutoff wavelength at the d/Λ values reported in Fig. 6. The mean values of V_1^* and V_2^*, respectively, 2.67 and 2.46, are also reported as solid lines in Fig. 9 and have been assumed as reference values like the 2.405 value of a standard fiber. Figures 10 and 11 show the V number versus the normalized wavelength calculated according to Eqs. (2) and (3) and the corresponding V^* mean value as an horizontal solid line. Of course, the crossings between the V^* line and the V-number curves for the two formulations give again the λ^*/Λ behavior versus d/Λ, that is, the single-mode–multimode phase diagram of Fig. 6.

Finally, it is important to notice that the value of V_1^* here evaluated for the square-lattice PCFs is lower than π, the value for the triangular PCFs,[11] which has been obtained with the same V-number expression and by looking at the second-order-mode field distribution on the fiber cross section.[11,22] In particular, it has been shown that in triangular PCFs the second-order-mode effective transverse wavelength, related to the dimension of the defect region where the mode fits in, is $\lambda_\perp^* \simeq 2\Lambda$ at the cutoff con-

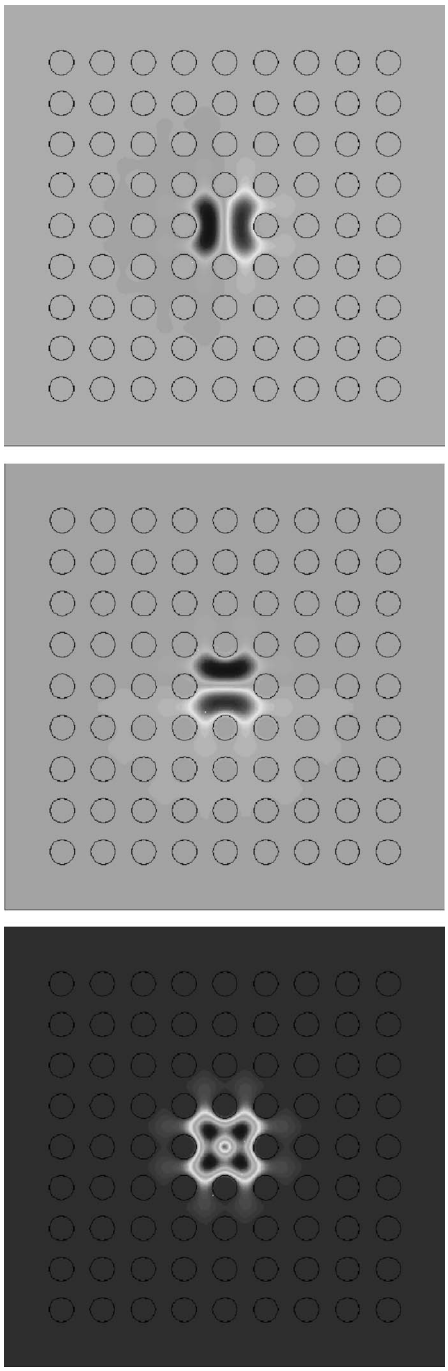

Fig. 12. H_x (top), H_y (middle), and intensity (bottom) distributions of the second-order guided mode at $\lambda/\Lambda \simeq 0.127$ for a four-ring square-lattice PCF with $d/\Lambda = 0.57$.

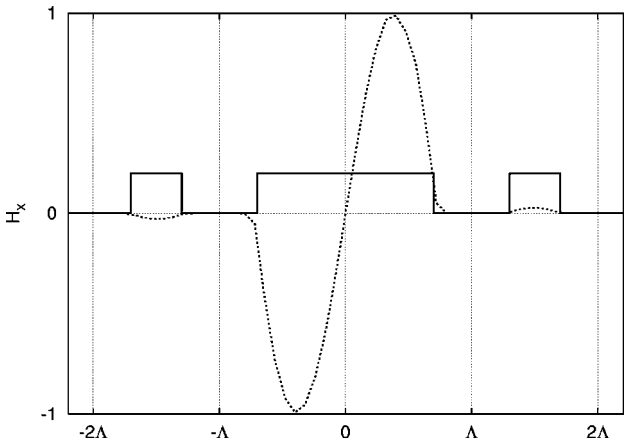

Fig. 13. Section of the square-lattice PCF cross section (solid curve) and of the H_x field component (dotted curve) along the x axis.

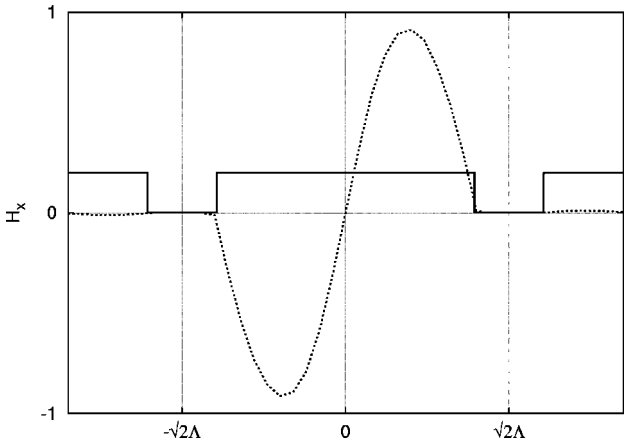

Fig. 14. Section of the square-lattice PCF cross section (solid curve) and of the H_x field component (dotted curve) along the 45° direction.

dition. As a consequence, the normalized cutoff frequency becomes $V_1^*=(2\pi/\lambda_\perp^*)\Lambda\simeq\pi$.[11] In order to extend the same approach to the square-lattice PCFs, one has to take the magnetic field components shown in Fig. 12 into account. It is important to underline that the field shape of the second-order mode in these PCFs is strongly influenced by the fourfold symmetry that characterizes the square lattice, in particular, by the position of the air holes belonging to the first ring. As a consequence, different $\lambda_\perp^*$ values can be obtained if the second-order-mode field amplitude is considered along the horizontal, or vertical, direction or along the 45° one. The two situations are depicted in Figs. 13 and 14. In the first case, the field shape is the same as the one reported for triangular PCFs,[11] so $\lambda_\perp^*\simeq 2\Lambda$ and $V_1^*\simeq\pi$. In contrast, if the 45° direction is considered, the separation between the first two null values of the second-order-mode field amplitude increases, as shown in Fig. 14, since the two opposite air holes belonging to the first ring are more distant. Thus $\lambda_\perp^*$ is higher, that is, $2\sqrt{2}\Lambda$, and, consequently, $V_1^*\simeq\pi/\sqrt{2}$. It is interesting to point out that the V_1^* value calculated in the present analysis, which is 2.67, is almost equal to the mean value between π and $\pi/\sqrt{2}$, which is 2.68. The corresponding $\lambda_\perp^*\simeq 2.34\Lambda$ is obtained by the mean value of the inverse of 2Λ and $2\sqrt{2}\Lambda$. In conclusion, it is not possible to simply extend the derivation of V_1^* previously proposed for triangular PCFs to the case of square-lattice PCFs, since a unique value of $\lambda_\perp^*$ cannot be easily found.

4. CONCLUSION

A thorough analysis has been performed on the cutoff properties of square-lattice PCFs by applying a method that involves the second-order-mode complex propagation constant. The single-mode–multimode phase diagram has been calculated, and it has been demonstrated that the single-mode operation region of square-lattice PCFs is wider than that of triangular ones. Moreover, it has been shown that square-lattice PCFs have also a larger endlessly single-mode operation region, $d/\Lambda<0.442$, compared with the one for triangular PCFs, which is smaller, being defined by $d/\Lambda<0.406$. Finally, the normalized cutoff frequency has been evaluated for square-lattice PCFs, and it has been demonstrated that V^* is lower than π, which is the value obtained for triangular fibers. The results presented in this paper suggest that square-lattice PCFs have interesting cutoff properties and can be successfully employed in applications that require large-mode-area fibers.

Corresponding author S. Selleri can be reached by phone, 39-0521-905763; fax, 39-0521-905758; or e-mail at stefano.selleri@unipr.it.

REFERENCES

1. A. Bjarklev, "Photonic crystal fibres and their applications," in *Proceedings of the European Conference on Optical Communications (ECOC)*, tutorial We3.3, pp. 324–347 (ECOC, 2003).
2. D. J. Richardson, W. Belardi, K. Furusawa, J. H. V. Price, A. Malinowski, and T. M. Monro, "Holey fibers: fundamentals and applications," in *Conference on Lasers and Electro-Optics*, Vol. 73 of 2002 OSA Technical Digest Series (Optical Society of America, 2002), pp. 453–454.
3. B. J. Eggleton, "Microstructured optical fibre devices," in *Proceedings of the European Conference on Optical Communications (ECOC)*, tutorial We3.2, pp. 200–233 (ECOC, 2004).
4. J. C. Knight, T. A. Birks, P. St. J. Russell, and D. M. Atkin, "All-silica single-mode optical fiber with photonic crystal cladding," Opt. Lett. **21**, 1547–1549 (1996).
5. T. A. Birks, J. C. Knight, and P. St. J. Russell, "Endlessly single-mode photonic crystal fiber," Opt. Lett. **22**, 961–963 (1997).
6. D. Ferrarini, L. Vincetti, M. Zoboli, A. Cucinotta, and S. Selleri, "Leakage properties of photonic crystal fibers," Opt. Express **10**, 1314–1319 (2002), http://www.opticsexpress.org/abstract.cfm?URI=OPEX-10-23-1314.
7. B. Kuhlmey, G. Renversez, and D. Maystre, "Chromatic dispersion and losses of microstructured optical fibers," Appl. Opt. **42**, 634–639 (2003).
8. L. Vincetti, "Confinement losses in honeycomb fibers," IEEE Photon. Technol. Lett. **16**, 2048–2050 (2004).
9. B. T. Kuhlmey, R. C. McPhedran, and C. Martijn de Sterke, "Modal cutoff in microstructured optical fibers," Opt. Lett. **27**, 1684–1686 (2002).
10. B. T. Kuhlmey, R. C. McPhedran, C. M. de Sterke, P. A. Robinson, G. Renversez, and D. Maystre, "Microstructured optical fibers: where's the edge?" Opt. Express **10**, 1285–1290 (2002), http://www.opticsexpress.org/abstract.cfm?URI=OPEX-10-22-1285.

11. N. A. Mortensen, J. R. Folkenberg, M. D. Nielsen, and K. P. Hansen, "Modal cutoff and the *V* parameter in photonic crystal fibers," Opt. Lett. **28**, 1879–1881 (2003).
12. P. St. J. Russell, E. Marin, A. Diez, S. Guenneau, and A. B. Movchan, "Sonic band gaps in PCF preforms: enhancing the interaction of sound and light," Opt. Express **11**, 2555–2560 (2003), http://www.opticsexpress.org/abstract.cfm?URI=OPEX-11-20-2555.
13. M. G. Franczyk, J. C. Knight, T. A. Birks, P. St. J. Russell, and A. Ferrando, "Birefringent photonic crystal fiber with square lattice," in *Lightguides and Their Applications II*, J. Wojcik and W. Wojcik, eds., Proc. SPIE **5576**, 25–28 (2004).
14. Y. Ni, Z. Lei, J. Shu, and P. Jiangde, "Dispersion of square solid-core photonic bandgap fibers," Opt. Express **12**, 2825–2830 (2004), http://www.opticsexpress.org/abstract.cfm?URI=OPEX-12-13-2825.
15. A. H. Bouk, A. Cucinotta, F. Poli, and S. Selleri, "Dispersion properties of square-lattice photonic crystal fibers," Opt. Express **12**, 941–946 (2004), http://www.opticsexpress.org/abstract.cfm?URI=OPEX-12-5-941.
16. Y. C. Liu and Y. Lai, "Optical birefringence and polarization dependent loss of square- and rectangular-lattice holey fibers with elliptical air holes: numerical analysis," Opt. Express **13**, 225–235 (2005), http://www.opticsexpress.org/abstract.cfm?URI=OPEX-13-1-225.
17. T. A. Birks, D. Mogilevstev, J. C. Knight, P. St. J. Russell, J. Broeng, P. J. Roberts, J. A. West, D. J. Allan, and J. C. Fajardo, "The analogy between photonic crystal fibres and step index fibres," in *Optical Fiber Communication Conference* (Optical Society of America, 1999), pp. 114–116.
18. N. A. Mortensen, "Effective area of photonic crystal fiber," Opt. Express **10**, 341–348 (2002), http://www.opticsexpress.org/abstract.cfm?URI =OPEX-10-7-341.
19. F. Brechet, J. Marcou, D. Pagnoux, and P. Roy, "Complete analysis of the characteristics of propagation into photonic crystal fibers, by the finite element method," Opt. Fiber Technol. **6**, 181–191 (2000).
20. M. Koshiba, "Full-vector analysis of photonic crystal fibers using the finite element method," IEICE Trans. Electron. **E85-C**, 881–888 (2002).
21. M. Koshiba and K. Saitoh, "Applicability of classical optical fiber theories to holey fibers," Opt. Lett. **29**, 1739–1741 (2004).
22. M. D. Nielsen and N. A Mortensen, "Photonic crystal fiber design based on the V-parameter," Opt. Express **11**, 2762–2767 (2003), http://www.opticsexpress.org/abstract.cfm?URI=OPEX-11-21-2762.
23. A. Ferrando, E. Silvestre, J. J. Miret, and P. Andrés, "Full-vector analysis of a realistic photonic crystal fiber," J. Opt. Soc. Am. A **17**, 1333–1340 (2000).
24. A. Cucinotta, S. Selleri, L. Vincetti, and M. Zoboli, "Perturbation analysis of dispersion properties in photonic crystal fibers through the finite element method," J. Lightwave Technol. **20**, 1433–1442 (2002)
25. T. P. White, B. T. Kuhlmey, R. C. McPhedran, D. Maystre, G. Renversez, C. M. de Sterke, and L. C. Botten, "Multipole method for microstructured optical fibers I. Formulation," J. Opt. Soc. Am. B **19**, 2322–2330 (2002).
26. T. P. White, B. T. Kuhlmey, R. C. McPhedran, D. Maystre, G. Renversez, C. M. de Sterke, and L. C. Botten, "Multipole method for microstructured optical fibers II. Implementation and results," J. Opt. Soc. Am. B **19**, 2331–2340 (2002).
27. S. G. Johnson and J. D. Joannopoulos, "Block-iterative frequency-domain methods for Maxwell's equations in a planewave basis," Opt. Express **8**, 173–179 (2001), http://www.opticsexpress.org/abstract.cfm?URI =OPEX-8-3-173.